Patterns of spiral wave attenuation by low-frequency periodic planar fronts

Miguel A. de la Casa and F. Javier de la Rubia
Departamento de Física Fundamental, UNED, 28040 Madrid, Spain

Plamen Ch. Ivanov[a)]
Center for Polymer Studies and Department of Physics, Boston University, Boston, Massachusetts 02215 and Institute of Solid State Physics, Bulgarian Academy of Sciences, 1784 Sofia, Bulgaria

(Received 17 August 2006; accepted 13 November 2006; published online 30 March 2007)

There is evidence that spiral waves and their breakup underlie mechanisms related to a wide spectrum of phenomena ranging from spatially extended chemical reactions to fatal cardiac arrhythmias [A. T. Winfree, *The Geometry of Biological Time* (Springer-Verlag, New York, 2001); J. Schutze, O. Steinbock, and S. C. Muller, Nature **356**, 45 (1992); S. Sawai, P. A. Thomason, and E. C. Cox, Nature **433**, 323 (2005); L. Glass and M. C. Mackey, *From Clocks to Chaos: The Rhythms of Life* (Princeton University Press, Princeton, 1988); R. A. Gray *et al.*, Science **270**, 1222 (1995); F. X. Witkowski *et al.*, Nature **392**, 78 (1998)]. Once initiated, spiral waves cannot be suppressed by periodic planar fronts, since the domains of the spiral waves grow at the expense of the fronts [A. N. Zaikin and A. M. Zhabotinsky, Nature **225**, 535 (1970); A. T. Stamp, G. V. Osipov, and J. J. Collins, Chaos **12**, 931 (2002); I. Aranson, H. Levine, and L. Tsimring, Phys. Rev. Lett. **76**, 1170 (1996); K. J. Lee, Phys. Rev. Lett. **79**, 2907 (1997); F. Xie, Z. Qu, J. N. Weiss, and A. Garfinkel, Phys. Rev. E **59**, 2203 (1999)]. Here, we show that introducing periodic planar waves with long excitation duration and a period longer than the rotational period of the spiral can lead to spiral attenuation. The attenuation is not due to spiral drift and occurs periodically over cycles of several fronts, forming a variety of complex spatiotemporal patterns, which fall into two distinct general classes. Further, we find that these attenuation patterns only occur at specific phases of the descending fronts relative to the rotational phase of the spiral. We demonstrate these dynamics of phase-dependent spiral attenuation by performing numerical simulations of wave propagation in the excitable medium of myocardial cells. The effect of phase-dependent spiral attenuation we observe can lead to a general approach to spiral control in physical and biological systems with relevance for medical applications.
 [DOI: 10.1063/1.2404640]

The dynamics of waves in excitable media[1–11] have been studied in physical, chemical, and biological systems under a variety of conditions including noise and inhomogeneities in the medium[12–14] and mechanical deformation.[15] Of particular interest is the problem of nonlinear wave interaction in the excitable medium of the heart muscle, as loss of wave stability and spiral wave breakup lead to spatiotemporal patterns associated with adverse cardiac events such as ventricular fibrillation and sudden cardiac death.[5,6,16,17] While different approaches to prevent spiral breakup have been proposed,[18–22] it is widely accepted that stable spiral waves cannot be suppressed by periodic planar wave fronts, since the frequency of the spiral is higher than the frequency of the fronts, and thus the domains of the spiral waves grow at the expense of the slower wave fronts.[7–11] Here, we focus on the attenuation of a single stable spiral wave. We show that it is possible to attenuate spiral waves by planar wave fronts with period longer than the rotational period of the spiral, and we address the problem of how to control spiral attenuation in excitable media. We find that when the fronts have long excitation duration, and are delivered at a specific phase relative to the rotational phase of the spiral, the spiral-front interaction is characterized by periodic patterns of spiral attenuation, which remain stable in time and over a broad range of physiologically meaningful parameter values. While spiral drift has been shown under similar conditions,[23] we do not aim to achieve spiral drift but to attenuate a stable spiral, i.e., to reduce the area covered by the spiral and the number of cells involved in the propagation of the spiral wave.

I. PHYSIOLOGICAL CONSIDERATIONS AND MODELING

We perform numerical simulations on a two-dimensional (2D) square lattice by considering interactions between the cells of the lattice, based on physiologically motivated rules representing the excitation dynamics of myocardial cells in the heart muscle (Fig. 1). The transmembrane potential of a myocardial cell represents the state of excitation of that cell. We model the state of the cell in position (i,j) in the lattice by an integer number E_{ij} as follows: (i) Resting (equilibrium) state: this state is represented in our model by $E_{ij}=0$, which corresponds to the experimentally observed transmembrane

a)Electronic address: plamen@buphy.bu.edu

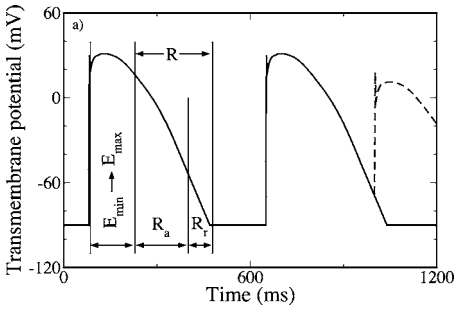

FIG. 1. Time evolution of the transmembrane potential of a ventricular myocite. After a superthreshold perturbation, the potential sharply increases from the resting state, of ≈−90 mV, to the excited state, with a plateau of positive potential of ≈30 mV. The duration of the excitation ranges from $E_{\min}$ to $E_{\max}$. The excited state is followed by a smooth decrease of the potential during the absolute refractory period, R_a. The decrease in the transmembrane potential continues during the relative refractory period, R_r, when a cell can be excited again but to a lower potential, and for shorter excitation duration compared to an excitation started during the resting state (dashed line).

potential ≈−90 mV.[24] A cell remains in the resting state for an unlimited time until a superthreshold perturbation occurs in the medium, which brings the cell to the excited state. This threshold for ventricular cells in guinea pigs was experimentally found to be ≈4–8 V/cm,[25] and is represented in our model by the parameter $\mathrm{Th}_{\mathrm{rest}}$ [Fig. 2(a)]. (ii) Excited state: when a cell enters the excited state, it takes a value in the interval $E_{\min} \leq E_{ij} \leq E_{\max}$, where $E_{\min} > 1$. For an excited

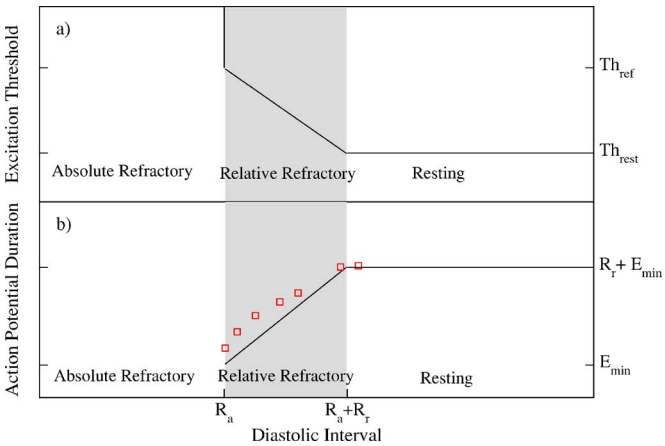

FIG. 2. Schematic presentation of the model. (a) Excitation threshold vs time past after the last excitation of a cell [also called diastolic interval (DI)]. For short DI, during the absolute refractory period, the cell cannot be excited and the excitation threshold is infinite. When the cell enters the relative refractory period, the excitation threshold is $\mathrm{Th}_{\mathrm{ref}}$, and with increasing DI the threshold decreases linearly in agreement with experimental observations (Ref. 29) until it reaches the value $\mathrm{Th}_{\mathrm{rest}}$ at the end of the relative refractory period. For long DI, during the resting state, the threshold remains constant and equal to $\mathrm{Th}_{\mathrm{rest}}$ (Ref. 27) We choose $\mathrm{Th}_{\mathrm{rest}}=20$ and $\mathrm{Th}_{\mathrm{ref}}=48$ to maintain the movement of the spiral tip in our simulations within a small area in agreement with experimental observations (Ref. 29). (b) Restitution curve—relation between the excitation duration [action potential duration (APD)] vs DI. There are no action potentials in the absolute refractory period. During the relative refractory period, the APD increases linearly with time, and in the resting state the APD is constant. We use the experimental restitution curve (denoted by □) and the conduction speed for guinea pig ventricular myocites (Ref. 29) to calibrate the parameter values, so that the restitution curve in our simulations reproduces the experimental one.

cell, in every time step τ, E_{ij} decreases by 1. Thus, in our simulations E_{ij} represents not only the transmembrane potential but also has a meaning of excitation duration [Fig. 2(b)], where at the beginning of the excitation the lowest excitation level a cell can assume is $E_{\min}$, corresponding to the shortest possible action potential duration (APD), while the highest excitation level is $E_{\max}$, which corresponds to the longest APD. At the end of the excitation period, $E_{ij}=1$ before the cell becomes absolute refractory. (iii) Absolute refractory state: when a cell enters this state, $E_{i,j}$ falls to $-R_a-R_r$, where R_a is the duration of the absolute refractory state when a cell cannot be excited. For an absolute refractory cell, in every time step τ, E_{ij} increases by 1. After R_a time steps, the cell becomes relative refractory (at $E_{ij}=-R_r$) before it reaches the resting state. (iv) Relative refractory state: this state is represented by $-R_r \leq E_{ij} \leq -1$, where R_r is the duration of the relative refractory state. A cell in this state can be excited with an excitation threshold experimentally observed to decrease in time as the cell approaches the resting state.[26] This threshold remains higher than the excitation threshold of cells in the resting state,[26] and in our model, it decreases linearly in time from the value $\mathrm{Th}_{\mathrm{ref}}$, when $E_{ij}=-R_r$, to the value $\mathrm{Th}_{\mathrm{rest}}$ in the resting state [Fig. 2(a)]. For every time step τ in which a relative refractory cell does not become excited, E_{ij} is increased by 1, until the cell reaches the resting state $E_{ij}=0$.

We define the excitation stimulus received by a cell in position (i,j) from the neighboring cells as $S_{ij}=\Sigma_{k,l}W_{kl}\sigma_{kl}$, where $k \in [i-\epsilon, i+\epsilon]$, $l \in [j-\epsilon, j+\epsilon]$, and ϵ defines the range of interaction. W_{kl} is a rotationally symmetric interaction kernel,[27] and $\sigma_{kl}=1$ if the cell in position (k,l) is excited and $\sigma_{kl}=0$ otherwise. To preserve a proper relation between the speed of propagation and the curvature of the wave front,[28] we set $\epsilon=5$. To account for the weaker effects of more distant neighbors, we choose values of the kernel elements W_{kl} decreasing with increasing distance from the center of the kernel.[27] A cell in position (i,j) that is excitable at time t will become excited in the next time step $t+1$ if it receives a stimulus S_{ij} larger than the excitation threshold of the cell. In this case, the new excited state of the cell is given by $E_{ij}^{t+1}=E_{ij}^{t}+R_r+E_{\min}$ [Fig. 2(b)], so that a cell at the beginning of the relative refractory state, with $E_{ij}^{t}=-R_r$, will reach an excitation level $E_{ij}^{t+1}=E_{\min}$. This is in accordance with the experimentally observed behavior of the restitution curve.[29] To account for the ion leakage from excited neighboring cells, we allow for an excitable cell to reach the longest APD, $E_{ij}^{t+1}=E_{\max}$, if (i) there is a cell (k,l) included in the kernel that is in the state $E_{kl}^{t}=E_{\max}$, and (ii) at the same time the perturbation S_{ij} is larger than the excitation threshold.

We consider a square lattice of $N \times N$ cells. To avoid effects of the lattice edge on the dynamics of wave propagation, and to account for experimental settings[30] we introduce no-flux boundary conditions, i.e., the lattice is surrounded by a strip of cells of width ϵ where the cells mirror the state of the cells neighboring the edge of the lattice.

The values of the parameters and the rules in our model match well the excitation dynamics in the ventricular cells of the guinea pig, traditionally used in experimental settings and theoretical studies:[29] (a) The experimentally observed

excitable gap (time between the end of the absolute refractory period and the next excitation) is $G=12\pm4$ ms,[29] which corresponds to one time step τ in our simulations, so we have $\tau=12$ ms; (b) comparing the experimental propagation speed of $v\approx75$ cm/s (Ref. 29) with the wave propagation of three lattice cells per time unit τ in our model, we have that our spatial unit is $\delta=0.3$ cm (≈100 myocite cells); (c) the experimentally found refractory period, $R^{\mathrm{exp}}=R_a^{\mathrm{exp}}+R_r^{\mathrm{exp}}\approx200$ ms, and relative refractory period $R_r^{\mathrm{exp}}\approx120$ ms,[29] are approximated in our simulation by the parameter values $R=R_a+R_r\in[18,30]$ and $R_r\in[7,10]$, in units of the time step τ; (d) the minimum and maximum APD experimentally observed are $E_{\mathrm{min}}^{\mathrm{exp}}\approx40$ ms and $E_{\mathrm{max}}^{\mathrm{exp}}\approx160$ ms,[29] which correspond to our parameters $E_{\mathrm{min}}\in[2,4]$ and $E_{\mathrm{max}}\in[10,20]$, in units of the time step τ; (e) the prolongation of the APD due to ion leakage has been physiologically estimated as $\Delta(\mathrm{APD})^{\mathrm{exp}}\approx D(\mathrm{APD})\partial_{xx}(\mathrm{APD})$, where $D\approx1$ cm^2/s is a diffusion constant.[31] Since typically $\mathrm{APD}\approx(E_{\mathrm{max}}^{\mathrm{exp}}+E_{\mathrm{min}}^{\mathrm{exp}})/2$ and $\partial_{xx}(\mathrm{APD})\approx(E_{\mathrm{max}}^{\mathrm{exp}}-E_{\mathrm{min}}^{\mathrm{exp}})/\delta^2$, we find $\Delta(\mathrm{APD})^{\mathrm{exp}}\approx130$ ms, which compares to the maximum prolongation in our model $\Delta(\mathrm{APD})^{\mathrm{model}}=E_{\mathrm{max}}-E_{\mathrm{min}}\in[6,18]$ in units of τ. The shape of the model restitution curve shown in Fig. 2(b) mimics the experimental data.[29] Thus, our model is based on experimentally relevant parameter values.

We generate the spiral according to a standard procedure, by propagating a planar front with one end close to the center of the lattice and the other end on the lattice edge.[32] We wait for 300 time steps τ (≈15 spiral rotations) until the spiral reaches a stable rotation with the tip moving only within a small approximately linear area of ≈30 cells near the center of the lattice, as observed in experimental settings.[33] We next introduce planar fronts with a period T, starting from the edge of the lattice. Each front is generated as a line of excited cells with maximum APD, $E_{1j}=E_{\mathrm{max}}$, for $j=1,\ldots,N$. To test whether it is possible to attenuate spiral waves with slow fronts, we choose the period T of the fronts to be longer than the rotational period of the spiral. We release the first front at time T_0 (in units τ) after the stabilization period of the spiral. The width of the front is proportional to the parameter E_{max} and to the speed of propagation, which depends on the excitation thresholds $\mathrm{Th}_{\mathrm{rest}}$ and $\mathrm{Th}_{\mathrm{ref}}$. Under these conditions, the position of the spiral tip remains stable and localized within a small area, and thus the patterns of spiral attenuation we find are not the result of spiral drift. To track if the spiral is attenuated, we follow the time evolution of every individual cell in the lattice. To survey the system, we also measure the total number of excited cells in the lattice as a function of time.

II. RESULTS

In contrast to previous studies showing that spiral waves cannot be attenuated by fronts of lower frequency,[7–11] we hypothesize that the interaction of a stable spiral wave and lower-frequency periodic planar fronts with sufficiently long excitation duration and with period T larger than the rotational period of the spiral can lead to spiral attenuation. Specifically, we hypothesize that spiral attenuation can only occur for an appropriate timing of the descending fronts (as measured by T_0) relative to the rotational phase of the spiral. We find that the interaction between the fronts and the spiral leads to complex patterns where, after several passing fronts, the spiral is attenuated (Fig. 3). These patterns repeat in time and remain stable for a broad range of physiologically meaningful parameter values (Fig. 7). Further, we find that the system exhibits a variety of different patterns that fall into two general classes: (i) Class I, where there is one spiral attenuation within a cycle of several passing fronts [Figs. 3(a)–3(c)], and (ii) Class II, where there are two nonconsecutive spiral attenuations within a cycle of several passing fronts [Figs. 3(d)–3(f)]. Repeating our simulations for $N=60,80,100,\ldots,200$, and for $N\times N$ and $N\times2N$ lattices, we find identical dynamics with the same periodic patterns of spiral attenuation. This also allows us to study the effect of the distance from the area where the fronts are introduced to the spiral core. In Fig. 4, we provide a color-coded representation of the spiral-front interaction on the lattice for the Class I and Class II patterns shown in Fig. 3.

The spatiotemporal patterns of spiral attenuation we present in Fig. 3 are a result of a complex nonlinear interaction between the spiral and the descending fronts. Without the fronts, the rotational period of the spiral is uniform in both space and time, i.e., the excitation of every cell in the lattice has a period equal to the rotational period of the spiral. In our simulations, the APD of a cell that becomes excited is $E_{ij}^{t+1}=E_{ij}^t+R_r+E_{\mathrm{min}}$. Since the excitable gap in experimental settings is $G\approx12$ ms,[29] which corresponds to one time step τ in our simulations, a cell in the relative refractory state $E_{ij}^t=-R_r$ is excited within a single time step to $E_{ij}^{t+1}=E_{\mathrm{min}}$. Thus, the APD of a cell in the isolated spiral is always E_{min}. The period of the spiral equals the sum of the duration of all states a cell undergoes during a single spiral rotation, $T_{sp}^-=E_{\mathrm{min}}+R_a+G$. In the presence of fronts, where the excited cells have maximum APD given by $E_{ij}=E_{\mathrm{max}}$, after a collision of a front with the spiral, a thin layer of maximum APD excitations propagates from the front along the advancing contour of the spiral (as shown in Fig. 5, frames 2–4). When these excitations reach the tip of the spiral before the next spiral rotation, the period of the spiral increases to $T_{sp}^+=E_{\mathrm{max}}+R_a+G$, which is also the period of the cells with maximum APD. In this situation, the spiral survives (Fig. 5, frame 6), and we observe a peak in the total number of excited cells in the lattice (Fig. 3). When the layer of cells with maximum APD excitations that propagates from the front to the spiral does not reach the tip of the spiral before the next spiral rotation (i.e., it does not cover the entire contour of the spiral), the period of the spiral remains T_{sp}^-. In this case, the cells at the tip of the spiral continue to have short APD given by $E_{ij}=E_{\mathrm{min}}$ (Fig. 5, frame 11). Due to the short APD, the spiral cannot propagate through the absolute refractory areas left by the layer of cells with long APD (given by $E_{ij}=E_{\mathrm{max}}$) formed between the front and the spiral, and the spiral is attenuated (Fig. 5, frame 12). This spiral attenuation corresponds to a reduced or absent peak in the total number of excited cells in the lattice (Fig. 3). In our simulations, the period of the fronts is $T=T_{sp}^++2$. Thus, the spiral attenuation we observe in Figs. 3 and 4 is achieved for planar fronts with a period longer than the period of the spiral.

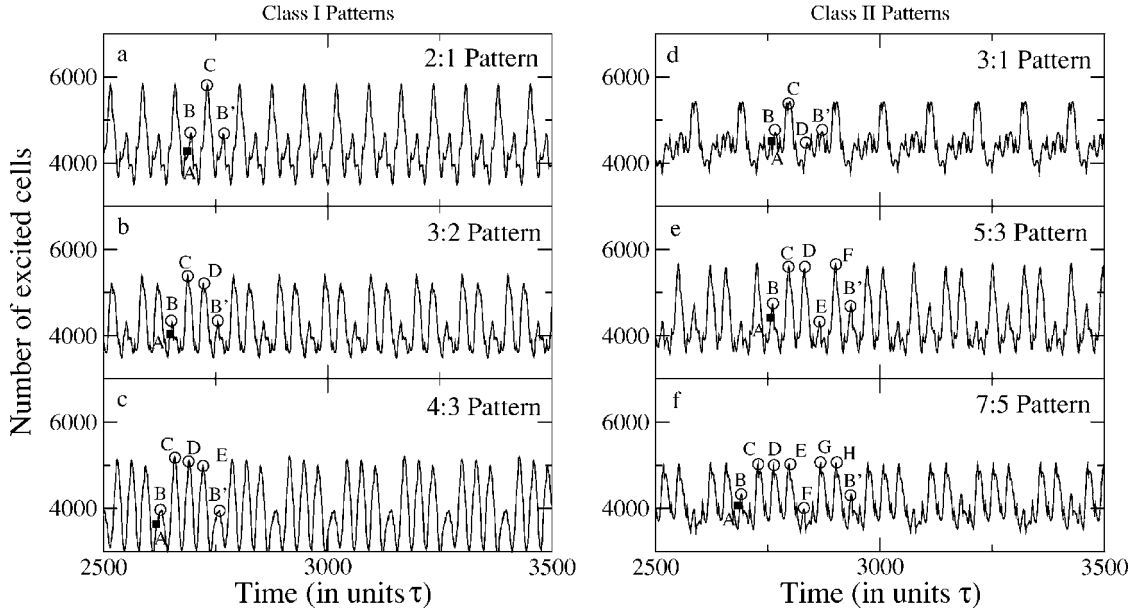

FIG. 3. Time evolution of the total number of excited cells from simulations on a square lattice of size $N=100$. Time is presented in units of the simulation time step τ. Data show a variety of robust patterns of spiral attenuation that remain stable in time. Absent and reduced peaks correspond to attenuation of the spiral. We find that these patterns belong to two general classes. (i) Class I $(n:n-1)$, where within a cycle of n fronts we have $n-1$ consecutive spiral rotations followed by one spiral attenuation. Examples of Class I patterns are presented in (a) pattern 2:1—out of the collision of the spiral with two consecutive fronts there is first a spiral attenuation (denoted by B) followed by one surviving spiral (denoted by C); (b) pattern 3:2—for each cycle of three consecutive fronts there is first a spiral attenuation (B) followed by two surviving spirals (C and D); (c) pattern 4:3—for each cycle of four consecutive fronts there is a spiral attenuation (B) and three surviving spirals (C, D, and E). The Class I patterns in (a), (b), and (c) are obtained for the following parameter values: $R_a=16$, $R_r=8$, $E_{\min}=2$, $E_{\max}=17,15,13$, $T_0=73,39,64$, respectively. (ii) Class II $(2n+1:2n-1)$, where within a cycle of $2n+1$ fronts there are $2n-1$ spiral rotations and two spiral attenuations. Examples of Class II patterns are presented in (d) pattern 3:1—for each cycle of three fronts there are two spiral attenuations (B and D) and one surviving spiral (C); (e) pattern 5:3—for each cycle of five fronts there are two spiral attenuations (B and E) and three surviving spirals (C, D, and F); (f) pattern 7:5—for each cycle of seven fronts we have two attenuations (B and F) and five surviving spirals (C, D, E, G, and H). The Class II patterns in (d), (e), and (f) are obtained for the following parameter values: $R_a=15,16,17$, $R_r=8$, $E_{\min}=2$, $E_{\max}=17,16,15$, $T_0=65,70,70$, respectively. In all panels, the instant in which a spiral attenuation is initiated is denoted by A, and the beginning of the next cycle is denoted by B', repeating the spiral attenuation in B. We find the same attenuation patterns independently of the size of the lattice and for a broad range of parameter values (Fig. 7).

We find that this mechanism of nonlinear interaction between the spiral and planar fronts comprised of cells with long APD and with frequency lower than the spiral rotation leads to the attenuation patterns in Figs. 3 and 4. We demonstrate that these patterns cannot be matched by a linear superposition of the number of excited cells of the isolated spiral and the number of excited cells in the isolated fronts, as we show in Fig. 6. Such a linear superposition exhibits periodic pulses with a higher number of excited cells, and cannot account for the missing peaks associated with spiral attenuation. Moreover, the pulses observed in the linear superposition of spiral and front form a cycle that repeats with a different duration compared to the duration of the cycle of spiral attenuation (Fig. 6).

Further, we observe that these complex front-spiral interactions lead to rich dynamics characterized by a variety of temporal patterns. We find that all patterns belong to two general classes. For Class I $(n:n-1)$ patterns, we observe that within a cycle of n fronts, we have $n-1$ slow spiral rotations with period T_{sp}^{+}, followed by two fast rotations with period T_{sp}^{-}:

$$\text{Class I:} \quad nT=(n-1)T_{sp}^{+}+2T_{sp}^{-}, \tag{2.1}$$

where the two fast rotations correspond to a single episode of spiral attenuation [Figs. 3(a)–3(c)].

For Class II $(2n+1:2n-1)$ patterns, we observe that within a cycle of $2n+1$ fronts, we have $2n-1$ slow spiral rotations, with period T_{sp}^{+}, and four fast rotations, with period T_{sp}^{-}:

$$\text{Class II:} \quad (2n+1)T=(2n-1)T_{sp}^{+}+4T_{sp}^{-}, \tag{2.2}$$

where the four fast rotations correspond to two separate nonconsecutive episodes of spiral attenuation [Figs. 3(d)–3(f)].

Solving for n in Eqs. (2.1) and (2.2), we obtain

$$\text{Class I:} \quad n=\frac{4T_{sp}^{-}-2T_{sp}^{+}}{2(T-T_{sp}^{+})}=\frac{1}{2}(2E_{\min}-E_{\max}+R_a+G), \tag{2.3}$$

$$\text{Class II:} \quad n=\frac{4T_{sp}^{-}-T_{sp}^{+}-T}{2(T-T_{sp}^{+})}=\frac{1}{2}(2E_{\min}-E_{\max}+R_a+G-1). \tag{2.4}$$

Based on the choice of parameter values for the system, the above expressions allow us to predict (i) the specific attenuation pattern, and (ii) the class to which a given pattern belongs. Parameter values for which we do not obtain integer n in either Eq. (2.3) or (2.4) cannot lead to spiral attenuation patterns. Thus, we can control the dynamical behavior of the

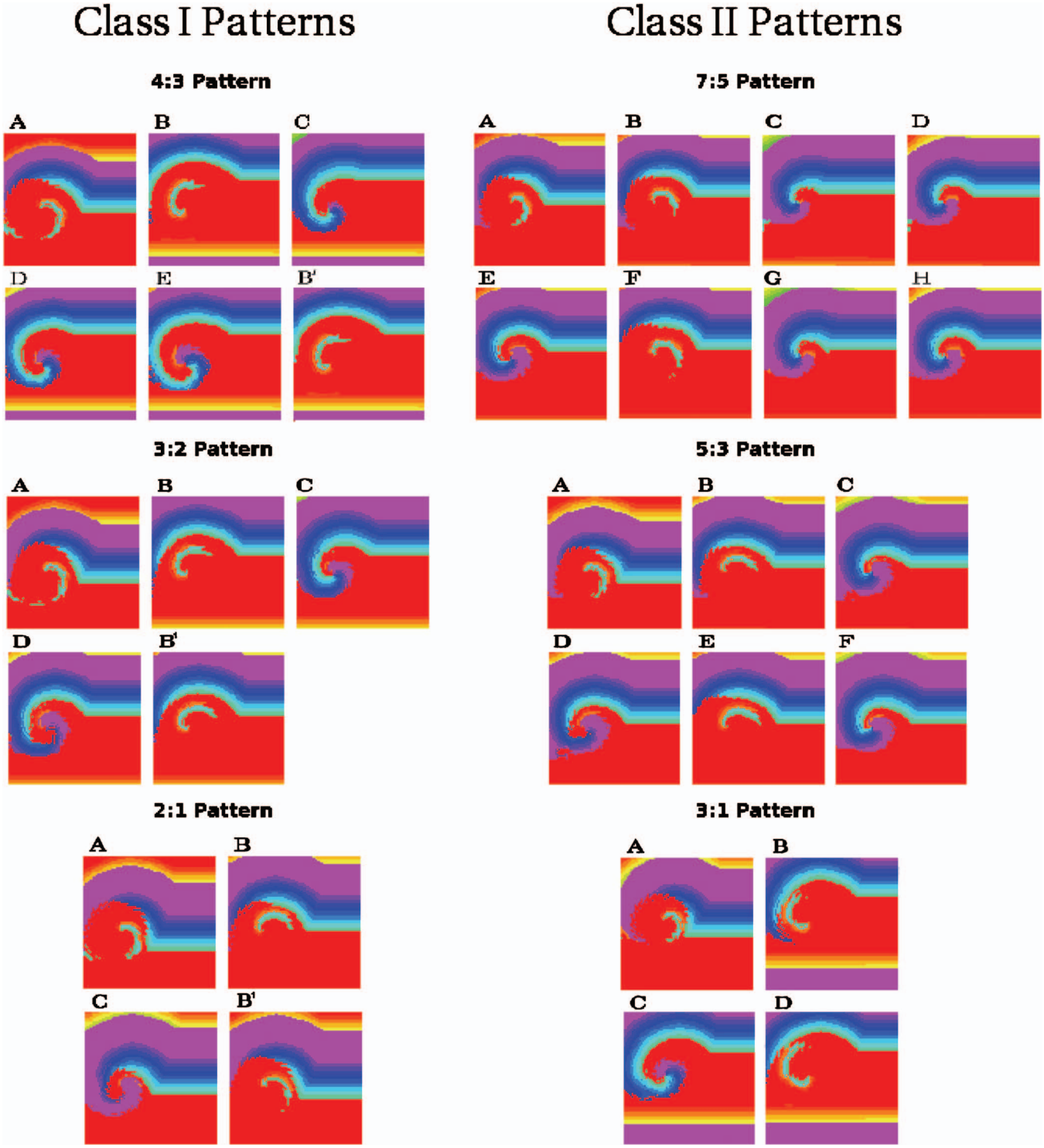

FIG. 4. (Color) Color-coded representation of the spiral-front interaction corresponding to the Class I and Class II patterns shown in Fig. 3. For increasing values of E_{ij} we have absolute refractory cells in red, relative refractory cells in orange and yellow, and excited cells in cyan, blue, and violet (highest values of E_{ij}). Snapshots for each pattern represent the same stages of the dynamics in time, as indicated by the corresponding capital letters in the panels of Fig. 3.

system in generating desired patterns of spiral attenuation.

Our simulations of up to 10^5 time steps τ (corresponding to $\approx$1500 seconds in experimental settings) show no change in the dynamics, which indicates that the spiral attenuation patterns remain stable in time. Further, we find that both Class I and Class II patterns can be obtained for a broad range of parameter values showing a robust effect of spiral attenuation. Specifically, we observe a particular structure in parameter space where individual patterns are organized along parallel straight lines, with every even line corresponding to a Class I pattern and every odd line corresponding to a Class II pattern (Fig. 7). This regular structure in parameter space is also predicted by Eqs. (2.3) and (2.4). In the upper left corner of the parameter diagram, for increasing values of R_a and decreasing values of $E_{\max}$, an attenuation becomes less frequent for increasing n, since we have only one attenu-

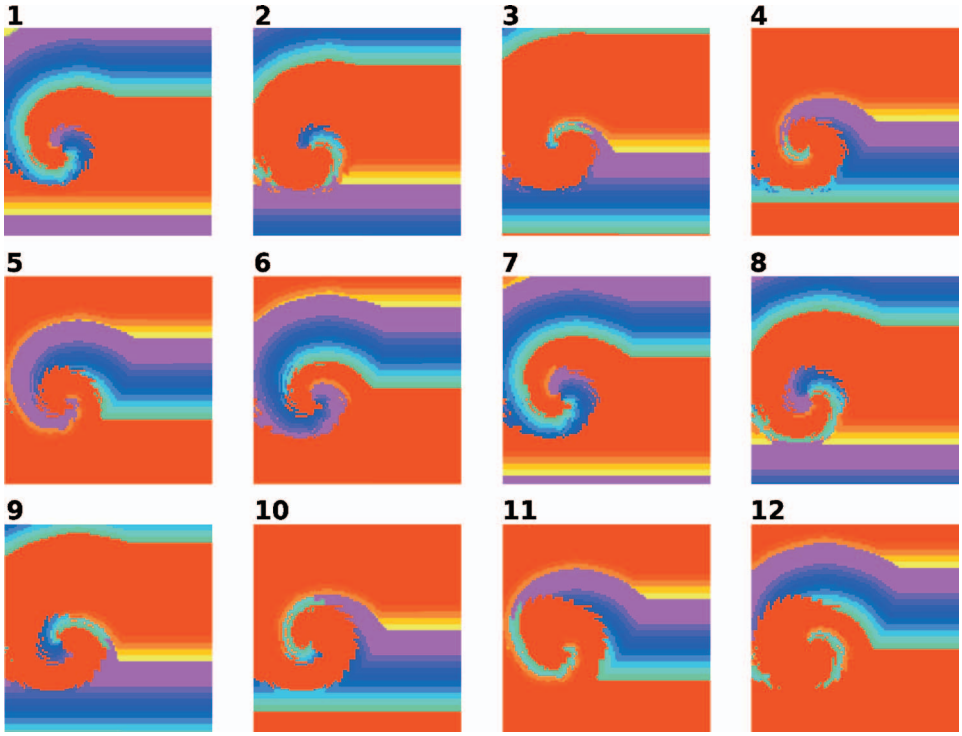

FIG. 5. (Color) Color-coded representation of the time evolution for the Class I 4:3 pattern obtained for the same parameter values as in Fig. 3(c). Snapshots represent the state of the lattice in intervals of five time steps τ. Snapshots 1, 7, and 12 correspond to D, E, and A in Fig. 3(c). For increasing values of E_{ij} we have absolute refractory cells in red, relative refractory cells in orange and yellow, and excited cells in cyan, blue, and violet (highest values of E_{ij}).

ation per cycle of n fronts for Class I patterns, and two attenuations per cycle for $2n+1$ fronts for Class II. In the upper right (large R_a and $E_{\max}$) and lower left (small R_a and $E_{\max}$) corners of the diagram, we find alternating patterns in a broad range of parameter values extending beyond the physiologically meaningful region (not shown in the diagram in Fig. 7). Finally, in the lower right corner of the diagram (small R_a and large $E_{\max}$) we do not observe patterns. This is in agreement with Eqs. (2.3) and (2.4), which do not allow $n<2$ for Class I (a cycle of at least two fronts is needed to have one attenuation within the cycle), and $n<1$ for Class II (a cycle of at least three fronts is needed to have two attenuations within the cycle).

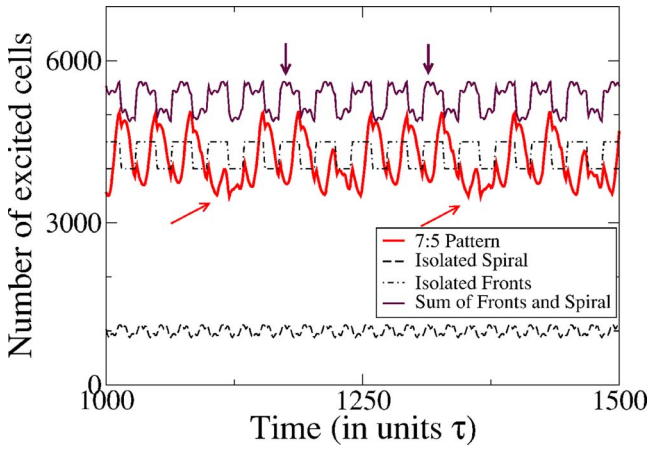

FIG. 6. Time evolution of the total number of excited cells in a square lattice of size $N=100$ for isolated fronts (without a spiral), isolated spiral (without fronts), linear superposition of fronts and spiral, and the Class II pattern 7:5, generated for the same parameter values as in Fig. 3(f) (arrows inclined to the right indicate one cycle of the 7:5 pattern). It is apparent that the 7:5 attenuation pattern cannot be a result of the linear superposition of periodic fronts and the spiral wave. This linear superposition is characterized by absence of attenuation, much higher average value of the number of excited cells, different profile of the periodic peaks, and shorter cycle (indicated by vertical arrows) compared to the 7:5 attenuation pattern, generated by the nonlinear interaction of the spiral wave and lower frequency fronts with maximum APD.

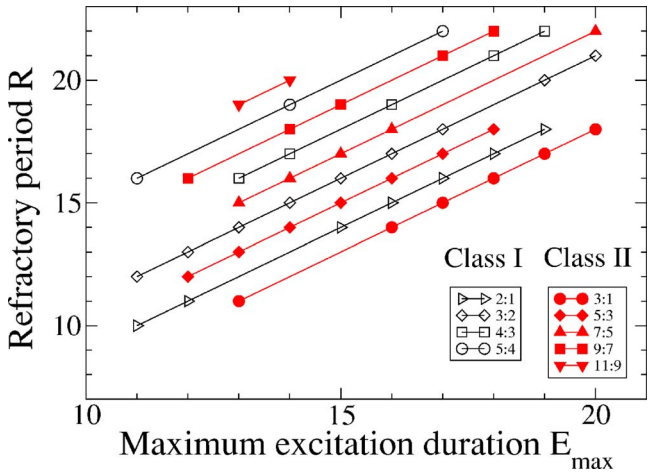

FIG. 7. Diagram of spiral attenuation patterns in parameter space R_a vs $E_{\max}$, for a square lattice of $N=100$ and fixed parameter values $R_r=8$ and $E_{\min}=2$. We observe attenuation patterns for a broad range of parameter values where each pattern can be found along a single straight line, in accordance with Eqs. (2.3) and (2.4). Patterns of Class I $(n:n-1)$ and Class II $(2n+1:2n-1)$ alternate in a series of parallel lines, where n increases with increasing R_a. To assess the intensity of the attenuation effect in different regions of the parameter diagram, we estimate for each cycle the ratio between the average number of excited cells when there is no spiral attenuation (large peaks in Fig. 3) and during spiral attenuation (reduced or absent peaks in Fig. 3). We find that this ratio is (i) characterized by a broad maximum in the central region of the parameter diagram and (ii) it exhibits a monotonic decrease in all directions of the parameter space for both classes of patterns, indicating a common behavior in the intensity of spiral attenuation.

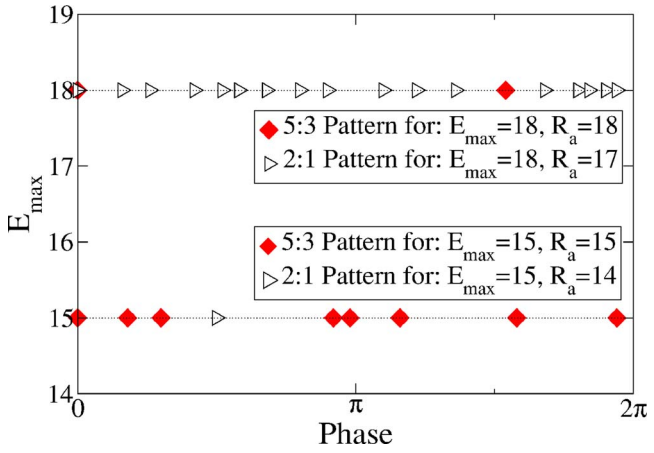

FIG. 8. Dependence of the attenuation patterns on the relative phase between the first released front and the spiral. Presented are only the patterns 2:1 (Class I) and 5:3 (Class II) for two sets of parameter values $E_{\max}$ and R_a, with the same symbols as in Fig. 7. Our results show that, for each set of parameter values on the diagram in Fig. 7, the patterns can appear only for specific values of the relative phase between the front and the spiral, indicating that the phase in which the front hits the spiral is crucial to achieve spiral attenuation.

We finally investigate how the front-spiral interaction depends on the relative phase between the spiral and the fronts. To answer this question, we perform several tests by releasing the first front at a time T_0 after the stabilization period of the spiral (which is 300 time steps τ), followed by a train of fronts with period T. We repeat the simulations for every value of $T_0 \in [0,T]$, for every point in the parameter space shown in Fig. 7. Surprisingly, we find that the patterns we observe in the parameter diagram of Fig. 7 occur only for specific values of T_0 (Fig. 8). For example, the Class I, 2:1 pattern generated for $E_{\max}=15$ and $R_a=14$ occurs only for phase $2\pi/4$, corresponding to $T_0=T/4$, while the same pattern, for $E_{\max}=18$ and $R_a=17$, occurs for several values of T_0 (Fig. 8). Thus, the observed dynamical patterns of spiral attenuation shown in Figs. 3 and 4 depend not only on the parameter values, but also on the relative phase between the spiral wave and the first released front. These findings indicate the presence of particular "vulnerable" phases during the spiral rotation when planar fronts can lead to spiral attenuation patterns.

III. SUMMARY

In summary, we find that the interaction of a spiral wave with planar fronts of sufficiently long excitation duration and a period longer than the period of the spiral can lead to spiral attenuation. The spiral attenuation only occurs for an appropriate timing of the descending fronts relative to the rotational phase of the spiral. This phase-dependent spiral attenuation is not a result of spiral drift and is characterized by different spatiotemporal patterns, each of them observed for a broad range of physiologically meaningful parameter values. Further, we find that these hitherto unknown patterns of phase-dependent spiral attenuation fall into two general classes, where each class is defined by a specific mathematical relation, and is represented by a structured diagram in parameter space. The spiral attenuation patterns we observe remain stable in time and do not change during the evolution of the system. These dynamics of phase-dependent spiral attenuation could be utilized for practical applications, and in the context of cardiac dynamics may lead to general approaches for controlling and preventing fatal arrhythmias.

ACKNOWLEDGMENT

Miguel de la Casa and Javier de la Rubia acknowledge partial support by the Ministerio de Educacion y Ciencia (Spain), Project No. FIS2005-01729, and Plamen Ch. Ivanov acknowledges support from NIH Grant No. 2RO1 HL071972.

[1] A. T. Winfree, *The Geometry of Biological Time* (Springer-Verlag, New York, 2001).
[2] J. Schutze, O. Steinbock, and S. C. Muller, "Forced vortex interaction and annihilation in an active medium," Nature (London) **356**, 45–47 (1992).
[3] S. Sawai, P. A. Thomason, and E. C. Cox, "An autoregulatory circuit for long-range self-organization in Dictyostelium cell populations," Nature (London) **433**, 323–326 (2005).
[4] L. Glass and M. C. Mackey, *From Clocks to Chaos: The Rhythms of Life* (Princeton University Press, Princeton, 1988).
[5] R. A. Gray, J. Jalife, A. V. Panfilov, W. T. Baxter, C. Cabo, J. M. Davidenko, A. M. Pertsov, P. Hogeweg, and A. T. Winfree, "Mechanism of cardiac fibrillation," Science **270**, 1222–1223 (1995).
[6] F. X. Witkowski, L. J. Leon, P. A. Penkoske, W. R. Giles, M. L. Spano, W. L. Ditto, and A. T. Winfree, "Spatiotemporal evolution of ventricular fibrillation," Nature (London) **392**, 78–82 (1998).
[7] A. N. Zaikin and A. M. Zhabotinsky, "Concentration wave propagation in two-dimensional liquid-phase self-oscillating system," Nature (London) **225**, 535–537 (1970).
[8] A. T. Stamp, G. V. Osipov, and J. J. Collins, "Suppressing arrhythmias in cardiac models using overdrive pacing and calcium channel blockers," Chaos **12**, 931–940 (2002).
[9] I. Aranson, H. Levine, and L. Tsimring, "Spiral competition in three-component excitable media," Phys. Rev. Lett. **76**, 1170–1173 (1996).
[10] K. J. Lee, "Wave pattern selection in an excitable system," Phys. Rev. Lett. **79**, 2907–2910 (1997).
[11] F. Xie, Z. Qu, J. N. Weiss, and A. Garfinkel, "Interactions between stable spiral waves with different frequencies in cardiac tissue," Phys. Rev. E **59**, 2203–2205 (1999).
[12] F. Moss, "Chemical dynamics—Noisy waves," Nature (London) **391**, 743–744 (1998).
[13] S. Kadar, J. C. Wang, and K. Showalter, "Noise-supported travelling waves in sub-excitable media," Nature (London) **391**, 770–772 (1998).
[14] A. Mikhailov and V. Zykov, "Rotating spiral waves in a simple model of excitable medium," Dokl. Akad. Nauk SSSR **286**, 341–344 (1986).
[15] M. P. Nash and A. V. Panfilov, "Electromechanical model of excitable tissue to study reentrant cardiac arrhythmias," Prog. Biophys. Mol. Biol. **85**, 501–522 (2004).
[16] A. T. Winfree, *When Time Breaks Down* (Princeton University Press, Princeton, 1987).
[17] H. M. Hastings, S. J. Evans, W. Q. Martha, L. Chong, and O. Nwasokwa, "Non-linear dynamics in ventricular fibrillation," Proc. Natl. Acad. Sci. U.S.A. **93**, 10495–10499 (1996).
[18] V. Petrov, V. Gáspár, J. Masere, and K. Showalter, "Controlling chaos in the Belousov-Zhabotinsky reaction," Nature (London) **361**, 240–243 (1993).
[19] V. S. Zykov, A. S. Mikhailov, and S. C. Müller, "Controlling spiral waves in confined geometries by global feedback," Phys. Rev. Lett. **78**, 3398–3401 (1997).
[20] S. J. Evans, H. M. Hastings, S. Nangia, J. Chin, M. Smolow, O. Nwasokwa, and A. Garfinkel, "Ventricular fibrillation: One spiral or many?," Proc. R. Soc. London, Ser. B **265**, 2167–2170 (1998).
[21] W. L. Ditto, M. L. Spano, V. In, J. Neff, and B. Meadows, "Control of human atrial fibrillation," Int. J. Bifurcation Chaos Appl. Sci. Eng. **10**, 593–601 (2000).
[22] S. Sitabhra, A. Pande, and R. Pandit, "Defibrillation via the elimination of spiral turbulence in a model for ventricular fibrillation," Phys. Rev. Lett. **86**, 3678–3681 (2001).

[23]G. Gottwald, A. Pumir, and V. Krinsky, "Spiral drift induced by stimulating wave trains," Chaos **11**, 487–494 (2001).
[24]G. W. Beeler and H. Reuter, "Reconstruction of the action potential of ventricular myocardial fibers," J. Physiol. (London) **268**, 177–210 (1977).
[25]V. Sharma, L. Susil, and R. Tung, "Paradoxical loss of excitation with high intensity pulses during electric field stimulation of single cardiac cells," Biophys. J. **88**, 3038–3049 (2005).
[26]*Essential Medical Physiology*, edited by L. R. Johnson (Lippincott-Raven, Philadelphia, 1998).
[27]V. G. Fast, I. R. Efimov, and V. I. Krinsky, "Transition from circular to linear rotation of a vortex in an excitable medium," Phys. Lett. A **151**, 157–161 (1990).
[28]V. S. Zykov, *Modeling of Wave Processes in Excitable Media* (Manchester University Press, Manchester, 1988).
[29]S. D. Girouard, "Optical mapping in a new guinea pig model of ventricular tachycardia reveals mechanisms for multiple wavelengths in a single reentrant circuit," Circulation **93**, 603–613 (1996).
[30]J. M. Starobin and C. F. Starmer, "Boundary-layer analysis of waves propagating in an excitable medium: Medium conditions for wave-front—Obstacle separation," Phys. Rev. E **54**, 430–437 (1996).
[31]A. Karma and F. Fenton, "Vortex dynamics in three-dimensional continuous myocardium with fiber rotation: Filament instability and fibrillation," Chaos **8**, 20–47 (1998).
[32]V. N. Biktashev and A. V. Holden, "Reentrant waves and their elimination in a model of mammalian ventricular tissue," Chaos **8**, 48–56 (1998).
[33]V. I. Krinsky, I. R. Efimov, and J. Jalife, "Vortices with linear cores in excitable media," Proc. R. Soc. London, Ser. A **437**, 645–655 (1992).